



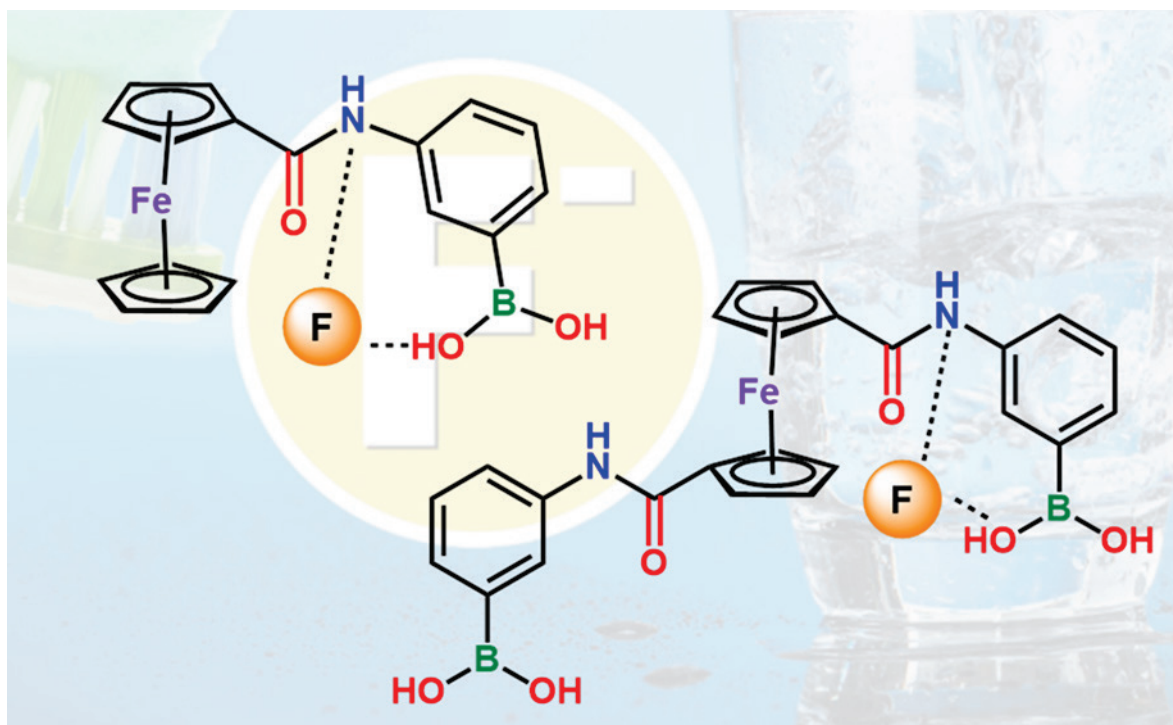
US Army Corps  
of Engineers®  
Engineer Research and  
Development Center



## Boronic Acid Functionalized Ferrocene Derivatives Towards Fluoride Sensing

P. U. Ashvin Iresh Fernando, Gilbert K. Kosgei,  
Matthew W. Glasscott, Garrett W. George, Erik Alberts,  
and Lee C. Moores

July 2022



**The U.S. Army Engineer Research and Development Center (ERDC)** solves the nation's toughest engineering and environmental challenges. ERDC develops innovative solutions in civil and military engineering, geospatial sciences, water resources, and environmental sciences for the Army, the Department of Defense, civilian agencies, and our nation's public good. Find out more at [www.erdclibrary.on.worldcat.org/discovery](http://www.erdclibrary.on.worldcat.org/discovery).

To search for other technical reports published by ERDC, visit the ERDC online library at <http://www.erdclibrary.on.worldcat.org/discovery>.

# **Boronic Acid Functionalized Ferrocene Derivatives Towards Fluoride Sensing**

Gilbert K. Kosgei, Matthew W. Glasscott, Garrett W. George, and Lee C. Moores

*US Army Engineer Research and Development Center (ERDC)  
Environmental Laboratory (EL)  
3909 Halls Ferry Rd  
Vicksburg, MS 39180-6199*

P. U. Ashvin Iresh Fernando

*Bennett Aerospace Inc.  
1100 Crescent Green #250  
Cary, NC 27518*

Erik Alberts

*SIMETRI  
7005 University Blvd.  
Winter Park, FL 32792*

## **Final Report**

Approved for public release; distribution is unlimited.

Prepared for Installation and Operational Environments  
3909 Halls Ferry Rd.  
Vicksburg, MS 39180

Under Program Element Number U452684  
Project Number 496992  
Task Number A1000

## Abstract

In this technical report (TR), a robust, readily synthesized molecule with a ferrocene core appended with one or two boronic acid moieties was designed, synthesized, and used toward F<sup>-</sup> (free fluoride) detection. Through Lewis acid-base interactions, the boronic acid derivatives are capable of binding with F<sup>-</sup> in an aqueous solution via ligand exchange reaction and is specific to fluoride ion. Fluoride binding to ferrocene causes significant changes in fluorescence or electrochemical responses that can be monitored with field-portable instrumentation at concentrations below the WHO recommended limit. The F<sup>-</sup> binding interaction was further monitored via proton nuclear magnetic resonance spectroscopy (<sup>1</sup>H-NMR). In addition, fluorescent spectroscopy of the boronic acid moiety and electrochemical monitoring of the ferrocene moiety will allow detection and estimation of F<sup>-</sup> concentration precisely in a solution matrix. The current work shows lower detection limit (LOD) of ~15 μM (285 μg/L) which is below the WHO standards.

Preliminary computational calculations showed the boronic acid moieties attached to the ferrocene core interacted with the fluoride ion. Also, the ionization diagrams indicate the amides and the boronic acid groups can be ionized forming strong ionic interactions with fluoride ions in addition to hydrogen bonding interactions.

**DISCLAIMER:** The contents of this report are not to be used for advertising, publication, or promotional purposes. Citation of trade names does not constitute an official endorsement or approval of the use of such commercial products. All product names and trademarks cited are the property of their respective owners. The findings of this report are not to be construed as an official Department of the Army position unless so designated by other authorized documents.

**DESTROY THIS REPORT WHEN NO LONGER NEEDED. DO NOT RETURN IT TO THE ORIGINATOR.**

# Contents

Abstract .....	ii
Figures and Tables .....	iv
Preface.....	vi
<b>1 Introduction.....</b>	<b>1</b>
1.1 Background .....	1
1.2 Objectives .....	1
1.3 Approach .....	1
<b>2 Experimental Methods .....</b>	<b>3</b>
2.1 Materials .....	3
2.2 Instruments.....	3
2.3 Synthetic procedure for 1 and 2 .....	3
2.4 <sup>1</sup> H NMR based detection methodology .....	5
2.5 Fluorescence based detection methodology .....	5
2.6 Electrochemical based detection methodology .....	6
<b>3 Results and Discussion .....</b>	<b>7</b>
3.1 Nuclear magnetic resonance (NMR) based characterization .....	7
3.2 Preliminary computational calculations .....	12
3.3 Evaluation of photophysical properties and related fluorescence based binding studies .....	14
3.4 Electrochemistry based fluoride ion detection .....	17
<b>4 Conclusions and Future work.....</b>	<b>22</b>
References .....	23
Acronyms and Abbreviations .....	24
Report Documentation Page.....	25

# Figures and Tables

## Figures

Figure 1. Synthetic procedure for the synthesis of 1 and 2. ....	4
Figure 2. Stoichiometric calculations for the reagents used during the synthesis of 1 and 2, 1a and 2a represents the in-situ acid chloride formation step and 1b and 2b corresponds to the functionalization with amino phenyl boronic acid to obtain the desired products. ....	5
Figure 3. $^1\text{H}$ NMR of 1. ....	7
Figure 4. Stacked $^1\text{H}$ -NMR of mono-functionalized ferrocene (1) and related starting materials in $\text{DMSO-d}_6$ . ....	8
Figure 5. $^1\text{H}$ -NMR of di-functionalized ferrocene (2) compound in $\text{DMSO-d}_6$ . ....	9
Figure 6. Stacked $^1\text{H}$ -NMR titration of 2 with TBAF in $\text{DMSO-d}_6$ . ....	10
Figure 7. (a) Boronic acid region for 2 and (b) boronic acid region for 1 with addition of fluoride in $\text{DMSO-d}_6$ (Concentrations of each spectra corresponds to the concentration values given in Figure 6 ranging from 0.500 M to 0.0292 M Fluoride ion concentration). ....	11
Figure 8. Stacked $^1\text{H}$ NMR for binding of fluoride (TBAF) with regards to 1- in the Amide region. ....	11
Figure 9. Delta chemical shift related to the addition of fluoride- in the Boronic acid region. ....	12
Figure 10. (a and c) - ball and stick model showing the binding sites of the fluoride ions for both mono- and di-functionalized ferrocene compounds, (b and d) - Potential ionization sites for both compounds, blue regions are indicated as the ionization sites. ....	13
Figure 11. Predicted HOMO-LUMO gaps and orbital energy diagrams for 1 (left) and 2 (right). ....	13
Figure 12. (a) Photoluminescent excitation (PLE) spectra (dashed) and UV Vis absorption (solid) for 1 (black) and 2 (red) (b) PLE (solid) and emission (dashed) spectra for 1 (black) and 2 (red). ....	14
Figure 13. (a) emission spectra for 1, (b) emission spectra for 2, and (c) emission spectra of 2 after exposure to ambient room light for several minutes. ....	15
Figure 14. All figures shows before and after light exposure towards 2, (a) Absorption spectra, (b) PLE spectra and (c) Emission spectra. ....	16
Figure 15. (a) Fluorescence quenching response towards various concentrations of fluoride ions, (b) Calibration curve for raw intensity response, (c) $F_0/F$ response towards addition of fluoride ions. ....	17
Figure 16. Cyclic voltammograms of Mono- (right) and Di- compounds (left), concentration was set to be 0.5 mM for both compounds and 0.1 mM TBAPF <sub>6</sub> was used, all CV was performed in acetonitrile solvent system. ....	18
Figure 17. CV (left) and DPV (right) for 1 and 2 in similar environments. ....	18
Figure 18. (a) and (b) DPV for binding of fluoride of 2 and 1, (C) and (D) Current vs. $\log [\text{F}^-]$ for 1 and 2. Concentrations plotted in log molar scale. ....	19
Figure 19. (a) Calibration curve for Di- and (b) calibration curve for mono- with the addition of Fluoride ions. ....	20
Figure 20. Comparison of bound and unbound peaks obtained via DPV for 1 and 2. ....	21

Tables

Table 1. Data obtained from the calibration curve for 1 and 2. Standard deviations were determined  
from \_10\_ samples/scans. ....20

## Preface

This study was conducted for the Environmental Quality and Installations Research Program under 489630, “Water Sensors.” The technical monitor was Dr. Lee Moores, Engineer Research and Development Center-Environmental Laboratory (ERDC-EL).

The work was performed by the Environmental Chemistry Branch (EPC) of the Environmental Processes Division (EP), ERDC-EL. At the time of publication, Ms. Amber L. Russell was Chief, EPC; Mr. Warren Lorentz was Chief, EP; and Dr. Elizabeth A. Ferguson, ETZ was the Technical Director for Installations and Operational Environments. The Deputy Directors of ERDC-EL were Dr. Brandon Lafferty and Dr. Jack Davis, and the Director was Dr. Edmund Russo.

COL Teresa A. Schlosser was Commander of ERDC, and Dr. David W. Pittman was the Director.



# **1 Introduction**

## **1.1 Background**

The selective recognition of particular anions in the presence of competitive contaminants is an ongoing chemical challenge for sensing (De Silva et al. 1997). The high level of fluoride found in industrial waste streams has been of interest to civil authorities (EPA 2000); and the military, due to fluorinated G-type chemical warfare agents such as sarin, soman, and cytosarin (Jang et al. 2015). Therefore, it is necessary to explore molecules capable of detecting fluoride ions both in an aqueous environment and in the aerosol phase.

In the current literature, boronic acid-based derivatives have been used in conjunction with amides as Lewis acid/base pairs to bind fluoride ions (Bresner et al. 2005; Hiromasa et al. 1996). These studies inspired the present work of combining boronic acid moieties with electroactive ferrocene molecules enabling electrochemical based detections. Two ferrocene molecules were attached to boronic moiety, one with ferrocene carboxylic acid and the other with ferrocene dicarboxylic acid, which have been previously reported. However, these molecules were used for saccharide detection and have not been utilized for fluoride detection (Saleem et al. 2016). The goal of evaluating both molecules for fluoride detection was to explore having dual functionality over singular functionality towards binding of fluoride ions.

## **1.2 Objectives**

This work seeks to explore fundamental approaches for detecting fluoride ions in the environment using an easily synthesizable ferrocene-boronic acid molecule. Characterization was performed using  $^1\text{H}$  and  $^{13}\text{C}$  Nuclear magnetic resonance (NMR) spectroscopy.  $^1\text{H}$ -NMR was used to monitor fluoride ions binding. In addition, fluoride detection using fluorescent quenching studies and electrochemistry was conducted.

## **1.3 Approach**

The mono- and di carboxylic acid ferrocene derivatives were converted into acid chlorides using thionyl chloride. The di/mono boronic acid functionalized ferrocenes were then synthesized by coupling ferrocene

carbonyl chloride with 3-Aminophenylboronic acid in the presence of triethylamine, a weak base, which also acts a catalyst for the reaction. The reactions were separated and purified using solvent extractions and flash column chromatography. Lastly, the pure compounds were tested for fluoride binding using tetrabutylammonium fluoride (TBAF) as the fluoride probe.

## 2 Experimental Methods

### 2.1 Materials

The reagents ferrocenecarboxylic acid 97%, 1,1'-ferrocenedicarboxylic acid 96%, 3-aminophenylboronic acid, thionyl chloride 97%, tetrabutylammonium fluoride, and triethylamine  $\geq 99.5\%$  were purchased from Millipore-Sigma (St. Louis, MO, USA). The LC-MS grade dichloromethane, acetonitrile, tetrahydrofuran, and ethyl acetate were purchased from Fisher Scientific (Hampton, NH, USA). And high-purity water was obtained from a Milli-Q system with a resistivity  $\geq 18.2 \text{ M}\Omega \text{ cm}^{-1}$ .

### 2.2 Instruments

Florescence quenching studies were performed using an FLS1000 Photoluminescence Spectrometer (Edinburgh Instruments Ltd, UK). NMR based experiments were performed using a Bruker AVANCE 300 MHz NMR spectrometer (Bruker Biospin, USA) at 25 °C.

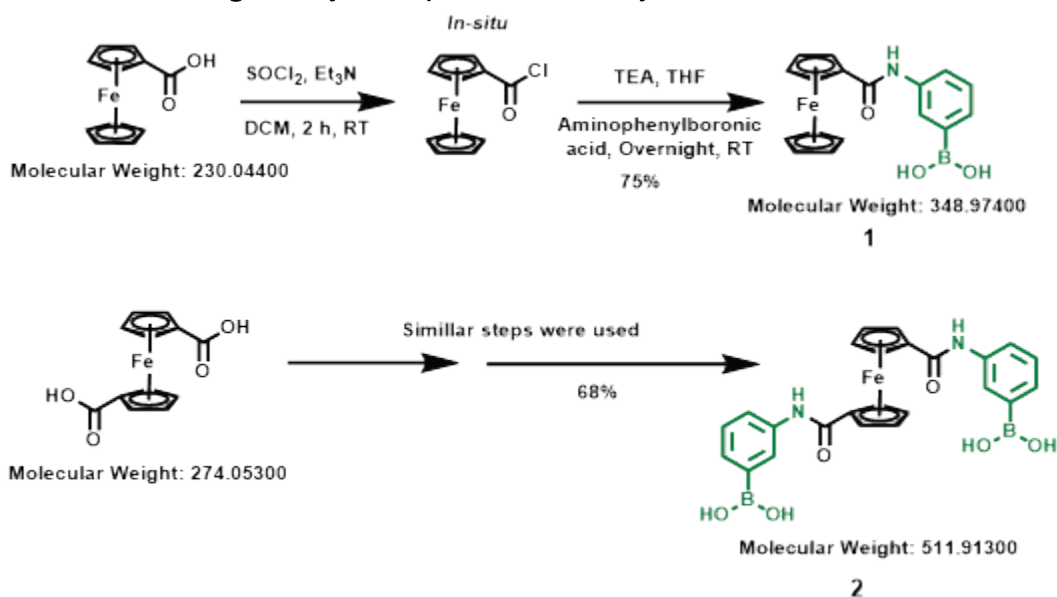
Electrochemical experiments were carried out using a BASi PalmSens 4 potentiostat (West Lafayette, IN, USA). PStrace software was used to facilitate all experiments. A gold disk working electrode (2 mm diameter), Ag/Ag<sup>+</sup> reference electrode with a Vycor frit, and a Pt wire counter electrode were used for all experiments. Electrodes were obtained from CH Instruments (Austin, TX, USA).

### 2.3 Synthetic procedure for 1 and 2

The synthetic procedure was a modification from the original work by Saleem et al. (2016). Ferrocene Di/Mono carboxylic acid was added to an oven dried, three-neck round bottom flask (RBF), followed with a 10xx-min nitrogen (N<sub>2</sub>) purge. Dry Dichloromethane (DCM) (dried over 3A molecular sieves) was added and thionyl chloride (SOCl<sub>2</sub>) was added in a single addition. The solution was then cooled to 0 °C and stirred magnetically for 10 min. Next, triethyl amine (TEA) dissolved in dry DCM was added dropwise. The reaction mixture was magnetically stirred at 0 °C for 90 min and another 30 min at room temperature. DCM was evaporated off by placing the reaction vessel above a water bath (60 °C) and fitted with a reflux condenser connected to vacuum. Once the DCM was evaporated, the reaction was purged with N<sub>2</sub> before 10 ml of

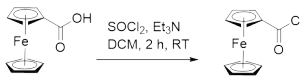
anhydrous tetrahydrofuran (THF) was added. The reaction was cooled back down to 0 °C. In a separate vial, 3-aminophenylboronic acid (3-APBA) and TEA were combined with THF. Ultra-sonication was performed (5-10 min), as 3-APBA is slightly soluble in THF. Using a syringe, the cloudy solution was added dropwise to the reaction vessel containing the ferrocene acid chloride. Finally, another 10 mL of dry THF was added and the reaction was magnetically stirred overnight at room temperature. To purify the product, 50 mL of Ethyl acetate (EtOAc) was added – as the  $\text{SOCl}_2$  reaction was performed *in situ*, black colored byproducts tend to form. The reaction mixture was filtered to remove the residue. The filtrate was transferred to a separatory funnel and washed with DI water 5 – 6 times to remove any unreacted materials. The organic layer was collected and dried over sodium sulfate ( $\text{Na}_2\text{SO}_4$ ) and the solvent was removed using a rotary evaporator. The purified product was analyzed by  $^1\text{H}$  NMR. This generalized procedure is shown in Figures 1 and 2 where Figure 1 corresponds to mono-functionalized ferrocene and Figure 2 is di-functionalized ferrocene.

Figure 1. Synthetic procedure for the synthesis of 1 and 2.

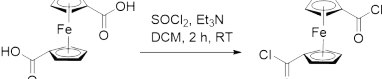


The following amounts of the reagents were used during the synthesis of the two-ferrocene based boronic acid derivatives.

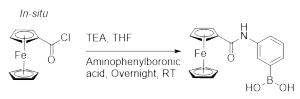
Figure 2. Stoichiometric calculations for the reagents used during the synthesis of 1 and 2, 1a and 2a represents the in-situ acid chloride formation step and 1b and 2b corresponds to the functionalization with amino phenyl boronic acid to obtain the desired products.

<b>1a</b> 		
Reactants/reagents	amount	mmol
Ferrocene carboxylic acid	500 mg	2.173
Thionyl chloride	250 $\mu$ l	3.259
Triethyl amine	630 $\mu$ l	4.346
Dry DCM	15 ml	n/a

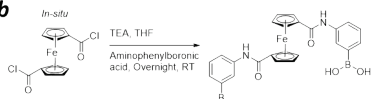
  

<b>2a</b> 		
Reactants/reagents	amount	mmol
Ferrocene di carboxylic acid	358.7 mg	1.302
Thionyl chloride	310 $\mu$ l	3.906
Triethyl amine	750 $\mu$ l	5.208
Dry DCM	12 ml	n/a

<b>1b</b> 		
Reactants/reagents	amount	mmol
Ferrocene acid chloride	540.8 mg	2.173
3-aminophenylboronic acid	300 mg	2.173
Triethyl amine	610 $\mu$ l	4.376
Anhydrous THF	40 ml	n/a

<b>2b</b> 		
Reactants/reagents	amount	mmol
Ferrocene di acid chloride	404.8 mg	1.302
3-aminophenylboronic acid	358.9 mg	2.604
Triethyl amine	550 $\mu$ l	3.946
Anhydrous THF	40 ml	n/a

## 2.4 $^1\text{H}$ NMR based detection methodology

50 mg of ferrocene di- or mono-carboxylic acid was dissolved in 600  $\mu$ L DMSO- $d_6$  and the concentration was maintained throughout the experiment. TBAF was dissolved in DMSO- $d_6$ . Fluoride ion concentrations in the NMR tube were changed sequentially from 0.029 M to 0.5 M s. The DMSO- $d_6$  residual solvent peak was used as the reference peak to observe chemical shift changes in the functionalized ferrocene compounds related to the addition of various amounts of TBAF.

## 2.5 Fluorescence based detection methodology

The FLS1000 Photoluminescence Spectrometer was used to measure photoluminescence excitation and emission spectra, quenching intensities, as well as decay curves to obtain the excitation lifetimes of the samples. The spectrometer is equipped with a mono-chromated 450 W ozone free xenon arc lamp as the excitation source, Photomultiplier tube - PMT-900 (185 nm – 900 nm), and NIR-PMTs (up to 1700 nm) as detectors from Hamamatsu. All spectra were automatically corrected for detector response.

## 2.6 Electrochemical based detection methodology

The electrode was polished with 1, 0.3, and 0.05  $\mu\text{m}$  alumina paste and cleaned with distilled water prior to use. It was also cycled between 1.95 and -0.35 V vs Ag/AgCl at 250 mV/s until a stable voltammogram was obtained to clean the gold surface. Cyclic voltammograms were carried out in acetonitrile with 0.1 M tetrabutylammonium perchlorate supporting electrolyte and 1 mM of the ferrocenyl compound of interest at a scan rate of 100 mV/s with a 1 mV increment. Differential pulse voltammetry was carried out in acetonitrile with 0.1 M tetrabutylammonium perchlorate and ~1 mM of the ferrocenyl compound from 0.2 - 0.8 V vs Ag/Ag<sup>+</sup> with the following parameters: equilibrium time: 10 sec, step potential 1 mV, pulse potential 50 mV, pulse time 25 ms, scan rate 20 mV/s. An Ag/Ag<sup>+</sup> reference electrode was used for all experiments in acetonitrile due to the instability of aqueous reference electrodes in organic solvent.

## 3 Results and Discussion

### 3.1 Nuclear magnetic resonance (NMR) based characterization

As shown in Figure 3, formation of the amide bond is observed, as amide protons are more shielded and are less exchangeable compared to carboxylic protons. The  $^1\text{H}$ -NMR of the starting material was stacked on the product to observe the up-field chemical shift and narrowing of the peak (Figure 4). When the boronic acid moiety is attached to ferrocene, the free movement of the amino phenyl boronic acid is restricted, which further resolves the phenyl protons. As the boronic acid molecule is freely rotating, an average splitting is seen, which is not as clearly resolved (Figure 4). Furthermore, one ferrocene proton peak is now more deshielded due to resonance effects from the amide exhibiting relatively lower resonance into the carbonyl oxygen compared to a carboxylic acid (orange arrows in Figure 4). Similarly, such chemical shifts are observed for the ferrocene di-boronic acid compound.

Figure 3.  $^1\text{H}$  NMR of 1.

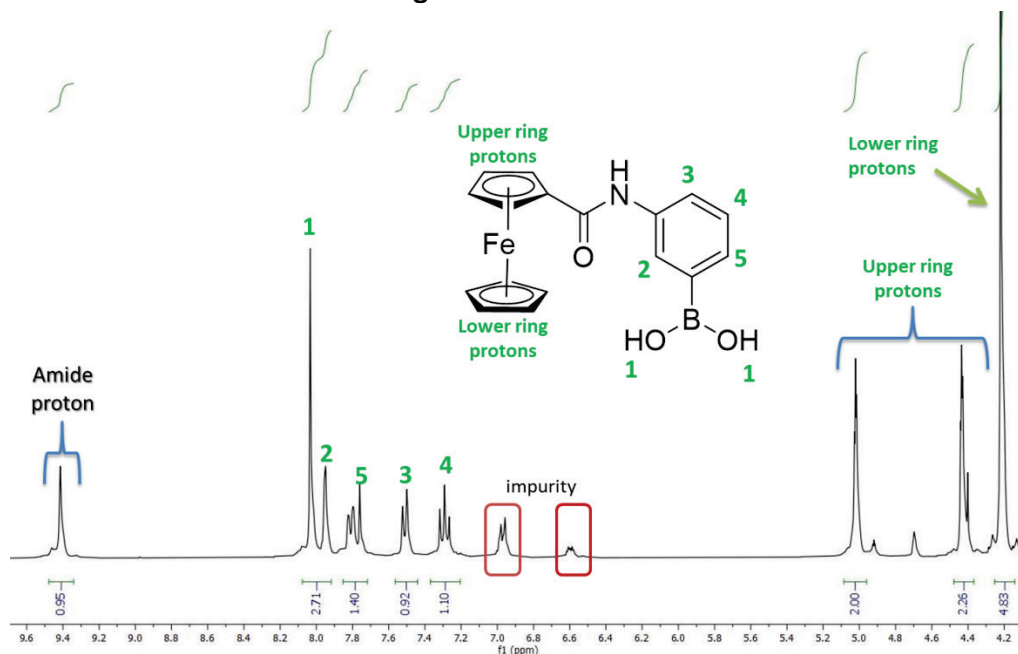


Figure 4 . Stacked  $^1\text{H}$ -NMR of mono-functionalized ferrocene (**1**) and related starting materials in  $\text{DMSO-d}_6$ .

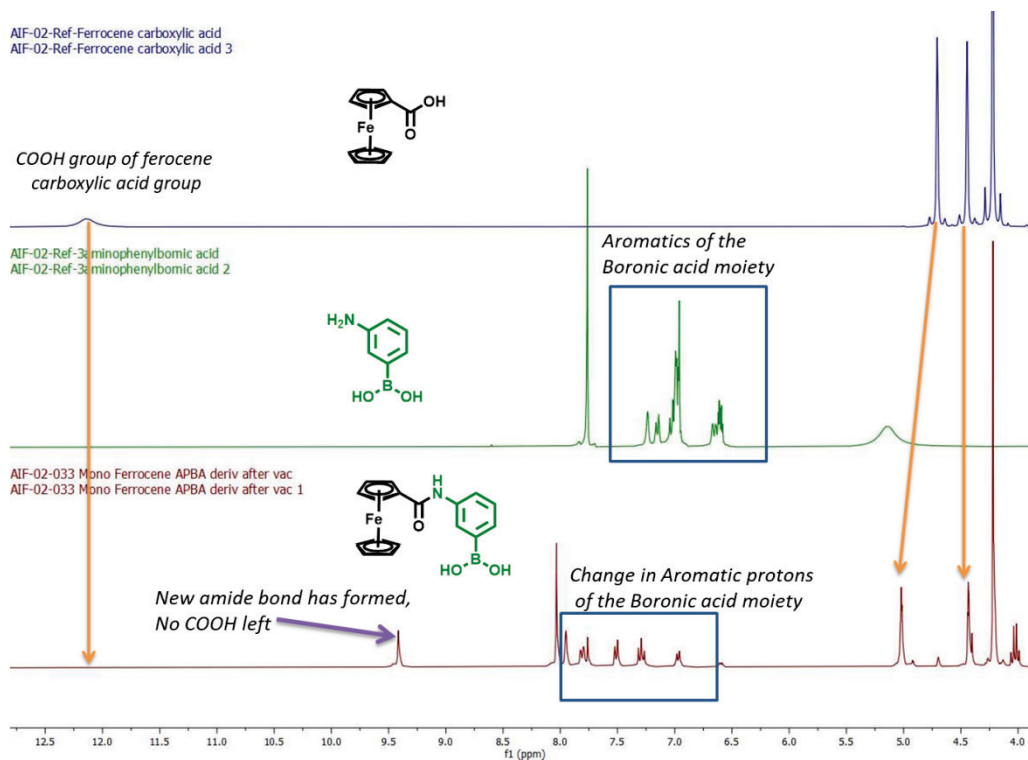
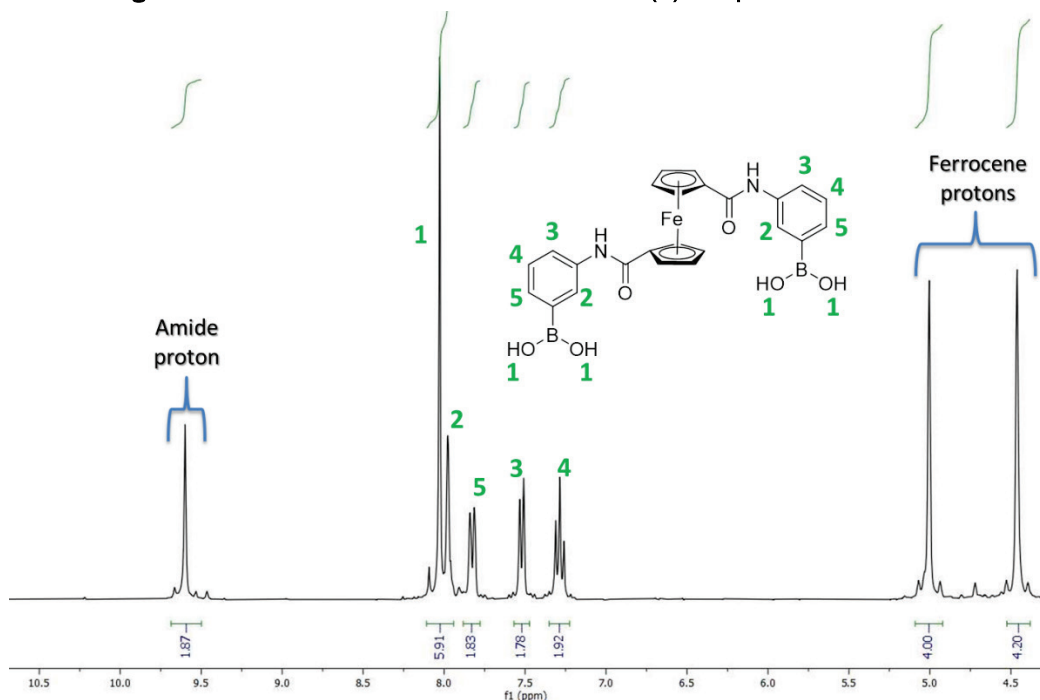


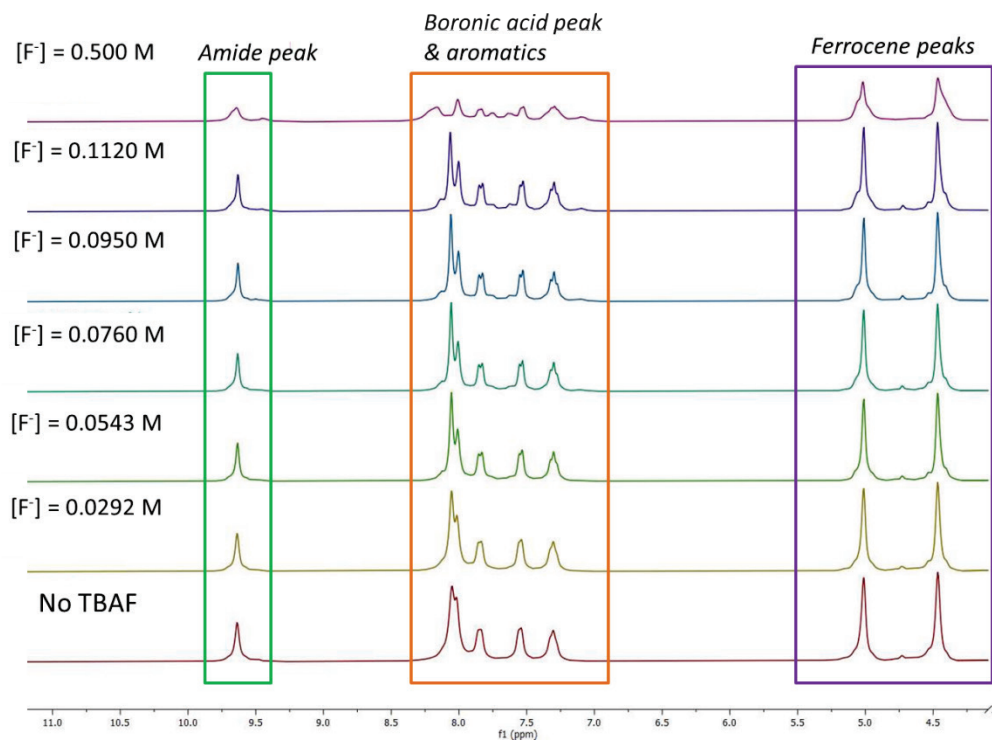
Figure 5 corresponds to the labeled  $^1\text{H}$  NMR spectrum of the di-functionalized compound. Since both cyclopentadiene groups are functionalized, there are only two ferrocene proton peaks observed since **2** is more symmetric compared to **1**. Also, the number of protons increased due to the attachment of two functional groups, which can be seen by an increase in the values given in the integrals.



Figure 5.  $^1\text{H}$ -NMR of di-functionalized ferrocene (2) compound in  $\text{DMSO-d}_6$ .

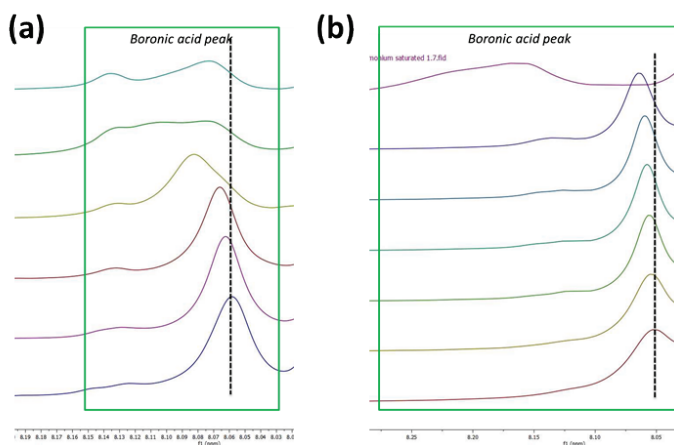


Once the molecules were synthesized, purified, and characterized, they were included in binding studies using TBAF observing the change in chemical shifts during  $^1\text{H}$ -NMR titrations. TBAF was used due to its solubility in organic solvents, compared to sodium fluoride or ammonium fluoride. For the  $^1\text{H}$ -NMR study, a concentration ranges from 0.029 M to 0.5 M, which served as the saturation point for the experiment, was used. The stacked NMR (Figure 6) shows the peaks tracked during the NMR titration studies for both molecules.

Figure 6. Stacked  $^1\text{H}$ -NMR titration of **2** with TBAF in  $\text{DMSO-d}_6$ .

The NMR titrations indicated that **1** exhibits higher chemical shift changes in all ranges compared to **2**. Except for the boronic acid region, all other regions did not show any chemical shift, or the chemical shift was extremely small in **2**. The boronic acid peak with the addition of higher amounts of fluoride shifted downfield, suggesting that boronic acid groups are coordinating with fluoride ions. However, as mentioned in Bresner et al. (2005), there were no synergetic effects from the amide group observed in **2**.

Figure 7. (a) Boronic acid region for **2** and (b) boronic acid region for **1** with addition of fluoride in DMSO- $d_6$  (Concentrations of each spectra corresponds to the concentration values given in Figure 6 ranging from 0.500 M to 0.0292 M Fluoride ion concentration).



This is different from the mono functionalized ferrocene compound, as all regions did show significant chemical shift changes except for the ferrocene peaks. The interaction with fluoride happens more than five bonds away from the ferrocene moiety, so this was expected. Delta chemical shift changes were plotted against the concentration of fluoride added for the boronic acid region. For **2**, the amide seems to be participating in the fluoride binding, as indicated by the chemical shift change to a more de-shielded region in the presence of an electronegative ion (fluoride). This indicates that **1** has a synergistic effect between the boronic acid moiety and the amide moiety to coordinate with the incoming fluoride ions.

Figure 8. Stacked  $^1\text{H}$  NMR for binding of fluoride (TBAF) with regards to **1**– in the Amide region.

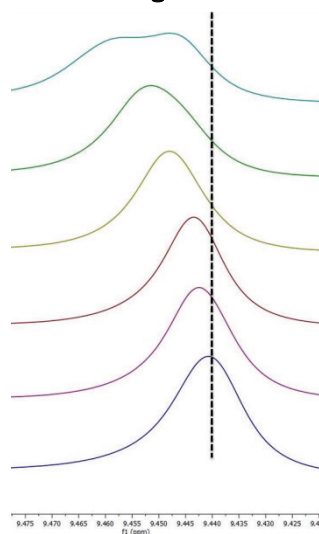
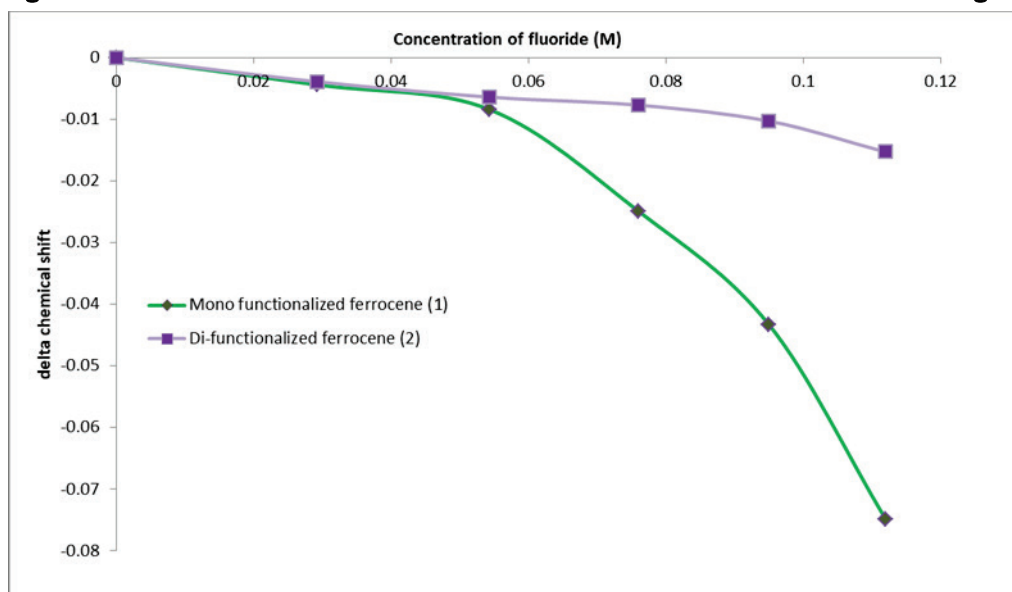


Figure 9. Delta chemical shift related to the addition of fluoride- in the Boronic acid region.



The delta chemical shift is significantly higher in **1** (Figure 9). In **2**, the boronic acid groups could interact with each other to block potential binding sites with the incoming fluoride ions, decreasing the overall binding effect. In **1**, the boronic acid and the amide groups are equally accessible to form a strong Lewis acid-base interaction system with the incoming fluoride ion.

### 3.2 Preliminary computational calculations

Preliminary computational work (using Spartan software) was performed to understand the binding mechanism of the mono and di-boronic acid compounds. For this work, molecular dynamics (MD) calculations were used to minimize the structure in the presence of fluoride, followed by semi-empirical PM3-level calculations for low-level energy minimization. It was visible that **1** and **2** interacted with the fluoride ion via the boronic acid moiety. It was also observed that when there were two fluoride ions, the di-functionalized compound wraps around the two arms. This type of interaction can take place within the molecule itself without the binding of fluoride. Due to the presence of Lewis acid and bases in both boronic acid moieties, Lewis acid-base interactions can take place within the molecule itself, which will cause the molecule to wrap around the ferrocene, blocking the fluoride from attaching. Further computational studies at a more accurate level of calculation are currently being pursued to understand this phenomenon.

Figure 10. (a and c) – ball and stick model showing the binding sites of the fluoride ions for both mono- and di-functionalized ferrocene compounds, (b and d) – Potential ionization sites for both compounds, blue regions are indicated as the ionization sites.

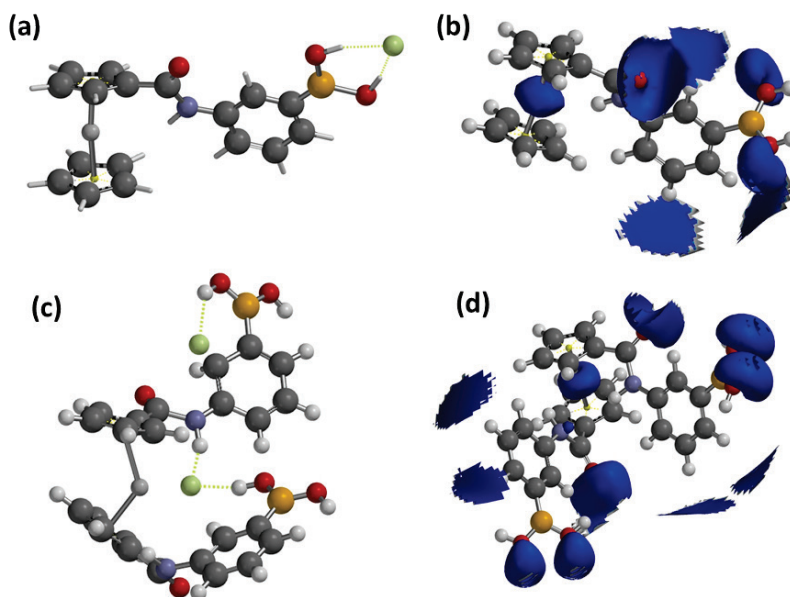
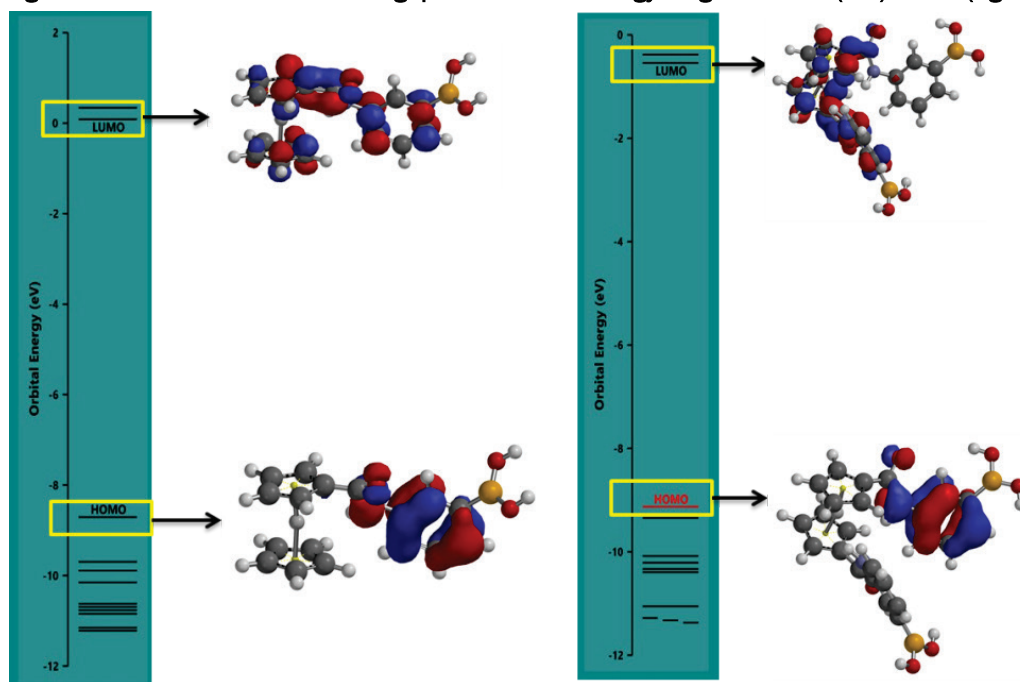


Figure 11. Predicted HOMO-LUMO gaps and orbital energy diagrams for **1** (left) and **2** (right).



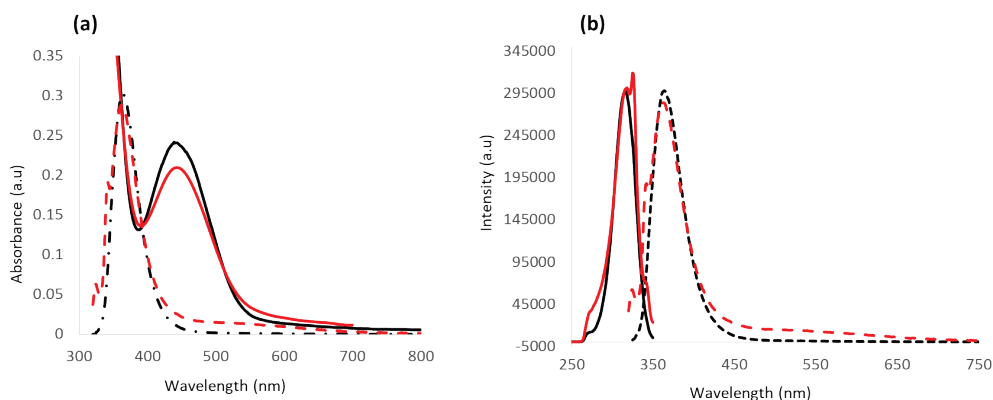
Ionization diagrams indicated the amides and the boronic acid groups form strong ionic and hydrogen bonding interactions with fluoride ions. Highest occupied molecular orbital (HOMO) and Lowest unoccupied molecular orbital (LUMO) gaps were identified to understand absorbance and emission studies. The addition of a second boronic acid moiety to **2**

causes a decrease in the HOMO energy level compared to the mono functionalized ferrocene. It also increases conjugation and thus decreases the energy gap.

### 3.3 Evaluation of photophysical properties and related fluorescence based binding studies

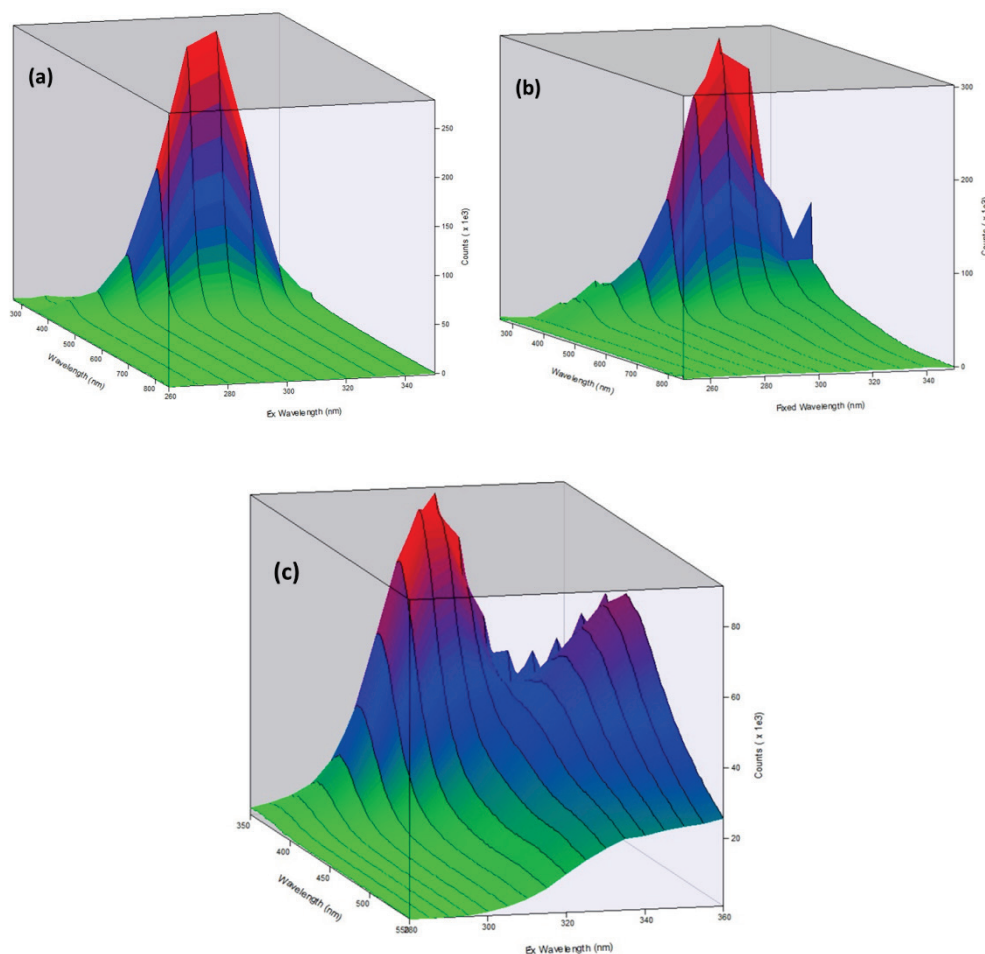
Examining the ground state absorption first for these compounds is important to facilitate emission studies. Therefore, UV-Vis absorption spectra were collected for both compounds.

Figure 12. (a) Photoluminescent excitation (PLE) spectra (dashed) and UV Vis absorption (solid) for **1** (black) and **2** (red) (b) PLE (solid) and emission (dashed) spectra for **1** (black) and **2** (red).



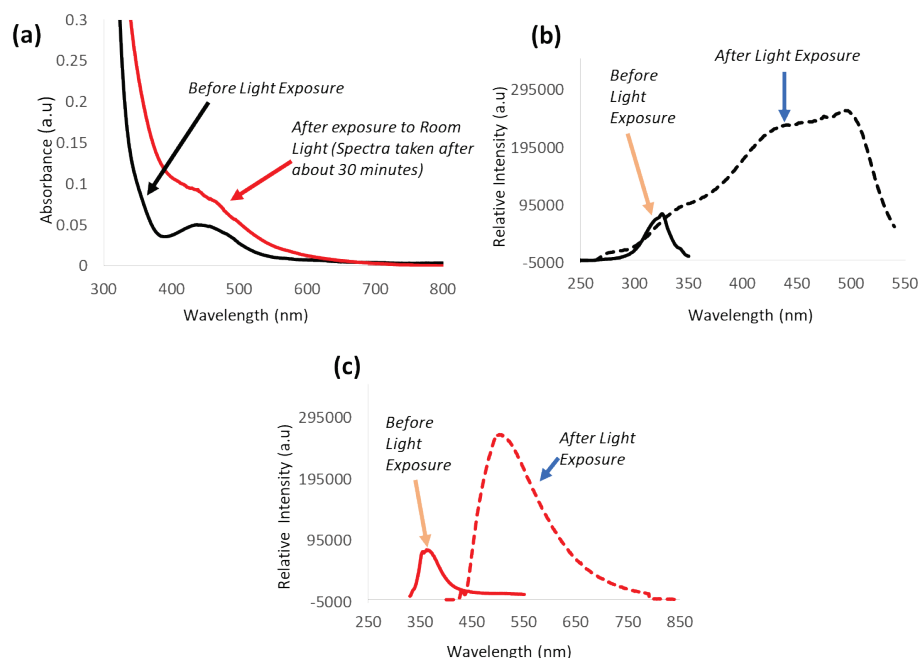
Both compounds exhibited an absorption maximum at 440 nm and an emission maximum around 360 nm. The additional pendent boronic acid moiety does not seem to bring any extra absorption bands or shifts in the absorption maxima compared to **1**. It was found that **1** was light-stable compared to **2**, which did not give emission consistent spectra after exposure to ambient light. This photo-instability was observed by forming an emissive iron complex appearing around 550 nm, which is not observed in **1** in similar conditions.

Figure 13. (a) emission spectra for 1, (b) emission spectra for 2, and (c) emission spectra of 2 after exposure to ambient room light for several minutes.



All Photoluminescence excitation (PLE) based spectra were monitored at 360 nm and scanned from 250 to 350 nm. To observe the additional emissive peak formation, spectra were monitored at 550 nm and excited from 250 to 540 nm. Therefore, it was apparent that **2** was light sensitive, and all other experiments were carried out in red-light conditions to avoid the formation of the additional emissive peak between 450 and 550 nm. To confirm the formation of this emissive complex, UV-Vis and emission spectra were also collected with exposure to ambient room light. Exposure to room light changed the absorption spectra (Figure 14a) and the PLE spectra had a greater intensity for the emissive band between 450 and 550 nm than the emissive band at 360 nm (Figure 14b). Furthermore, the emission spectra indicates that after light exposure, the band at 500 nm has increased almost five times compared to the band that was present around 360 nm with the absence of light (Figure 14c).

Figure 14. All figures shows before and after light exposure towards **2**, (a) Absorption spectra, (b) PLE spectra and (c) Emission spectra.

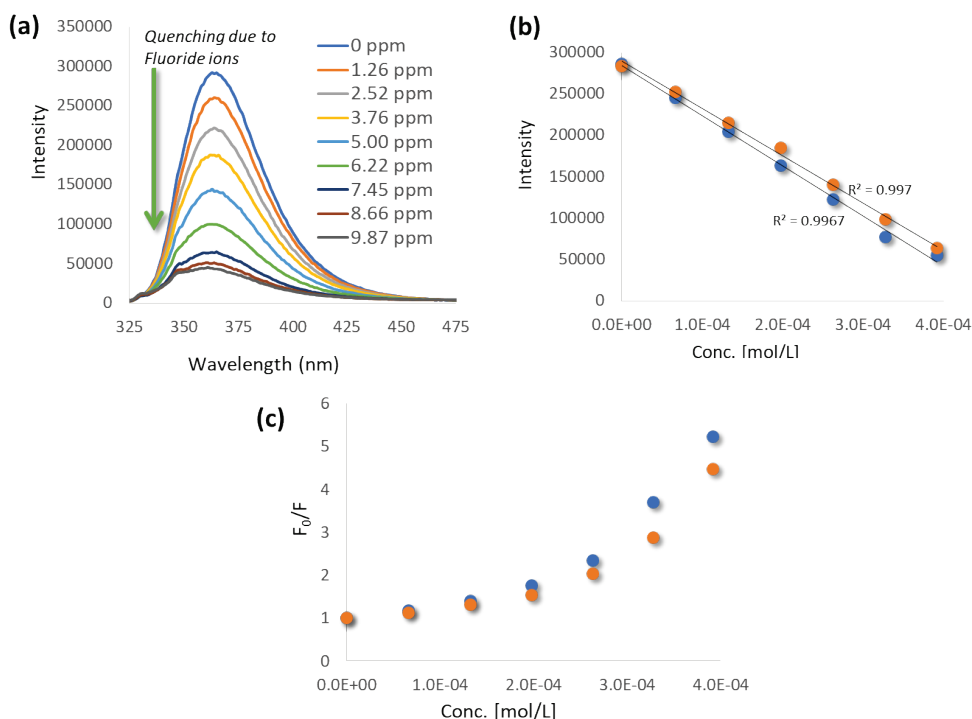


The rationale behind this phenomenon is that processes, such as deactivation, are taking place within **2**. Deactivation is usually through low-lying metal-centered energy states, which result in inefficient electron-transfer reactivity and a complete lack of photoluminescence. The resulting complex from **2** after light exposures seems to suppress such deactivation as shown by the spectra in Figure 14c. Therefore, it is possible that a photo-decomposition product might have formed resulting in the emission observed after exposure of **2** to ambient light. This led to using only **1** in the rest of emission studies related to fluoride detection.

TBAF was used for fluoride-based binding studies. It was observed that with addition of fluoride ions, the fluorescence emission decreased, showing a quenching response due to binding/interaction with incoming fluoride ions. The concentration range observed for binding phenomena was between 1 ppm and 10 ppm. A linear response was detected for this range of concentrations. When the response was converted into  $F_0/F$ , the response resulted in a logarithmic trend.



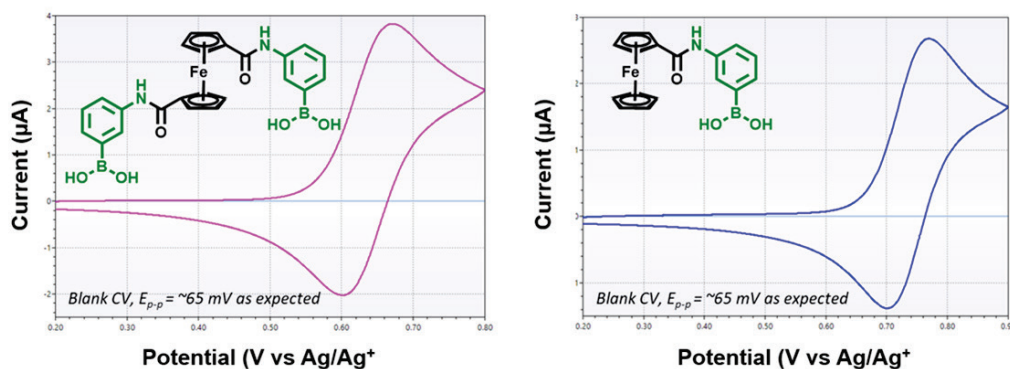
**Figure 15.** (a) Fluorescence quenching response towards various concentrations of fluoride ions, (b) Calibration curve for raw intensity response, (c)  $F_0/F$  response towards addition of fluoride ions.



### 3.4 Electrochemistry based fluoride ion detection

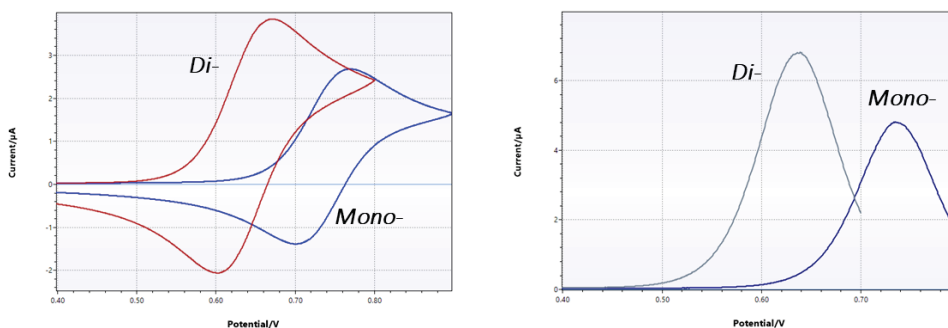
Ferrocene is a well-known electroactive species which is regularly used in electrochemical detection platforms. Hence, the goal of this work was to use the two ferrocene functionalized molecules in an electrochemical environment to elucidate their binding properties with respect to fluoride ions. Both compounds were analyzed using cyclic voltammetry (CV) and differential pulse voltammetry (DPV). 0.1 M TBAPF<sub>6</sub> was used as the supporting electrolyte. A gold disk working electrode (2 mm diameter), an Ag/Ag<sup>+</sup> reference electrode with a Vycor frit, and a Pt wire counter electrode were used for all experiments. Both **1** and **2** resulted in a peak-to-peak potential value of 65 mV, which is reasonably close to the 59-mV peak splitting predicted by the Nernst equation for 1-electron, outer sphere compounds (Figure 16).

Figure 16. Cyclic voltammograms of Mono- (right) and Di- compounds (left), concentration was set to be 0.5 mM for both compounds and 0.1 mM TBAPF<sub>6</sub> was used, all CV was performed in acetonitrile solvent system.



In comparison, it was found that **2** has more electron-donating ability and is therefore easier to oxidize. This may be related to conformational changes the addition of the second boronic acid group introduces and will be the subject of future investigation via molecular modeling. This is possibly due to the di-functionalization adding electron density to the redox-active iron center. This was indicated by the 100-mV difference in half wave potential observed in both CV and DPV (Figure 17).

Figure 17. CV (left) and DPV (right) for 1 and 2 in similar environments.



Monitoring the fluoride binding was conducted using DPV, where two peaks, possibly related to the bound and unbound fraction of the ferrocene compound, were observed. This phenomenon was exhibited by both **1** and **2**. It was found that after 10 μM of fluoride ions were added, the bound peak (at 520 mV) started to rise, while the unbound peak (635 mV) decreased. This phenomenon was observed for both compounds, only the location of the peak was changed as seen in Figure 18.

Figure 18. (a) and (b) DPV for binding of fluoride of 2 and 1, (C) and (D) Current vs. log [F<sup>-</sup>] for 1 and 2. Concentrations plotted in log molar scale.

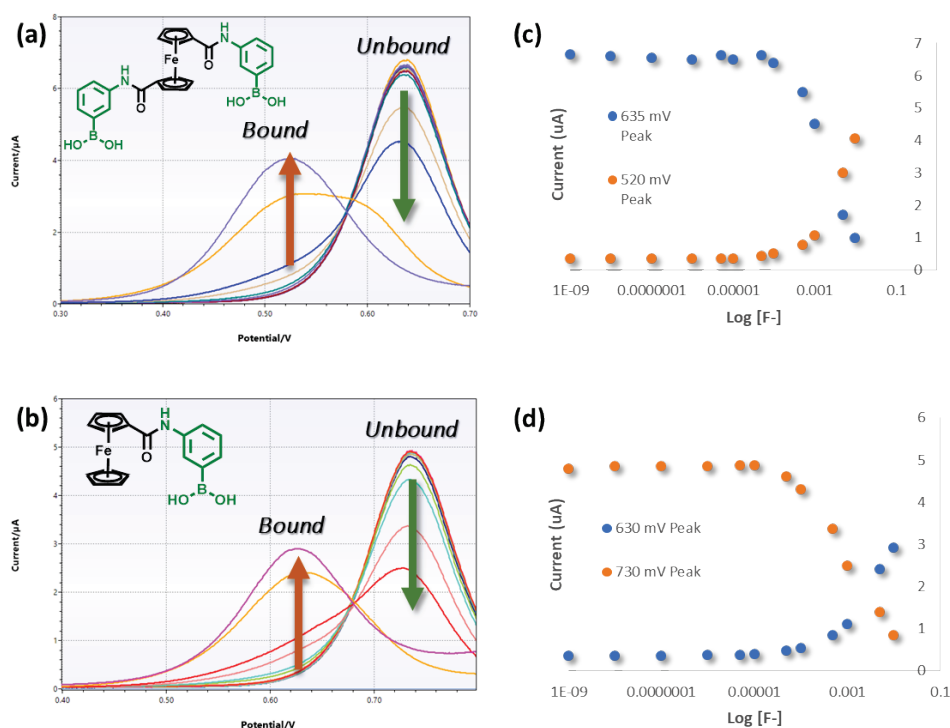


Figure 19 shows both compounds binding with fluoride ions in a similar fashion with a LOD of  $\sim 15 \mu\text{M}$  ( $285 \mu\text{g/L}$ ). Notably, it appears both peaks have a cross-over point at  $\sim 2 \mu\text{A}$ . It is unclear if these points represent anything (isosbestic, etc.) due to the fact that the peak height is based on parameters other than concentration (as in UV-vis for isosbestic analysis). Here, there are kinetic parameters at play (diffusion, charge transfer) which may differ between the two compounds. The concentrations are in log (M); additional data is shown in Table 1. LODs were calculated based on the standard deviation of the signal noise (y-residuals) (Shrivastava and Gupta 2011).

Assuming a liquid volume of 5 mL (as was used in this study), the mass of analyte necessary to render a response may be calculated using the LOD. This value, 75 nanomols, is equivalent to  $1.4 \mu\text{g}$  of fluoride. Taking sarin ( $140 \text{ g/mol}$ , 13.6% fluoride w/w), the LOD may then be extrapolated to needing only  $\sim 10 \mu\text{g}$  of sarin to diffuse into the matrix, hydrolyzed, and positively identified by the electrochemical process. It is estimated that 28-35  $\text{mg/m}^3$  is needed for a lethal dose, making this a potentially powerful sensing platform for chemical warfare agents.

Figure 19. (a) Calibration curve for Di- and (b) calibration curve for mono- with the addition of Fluoride ions.

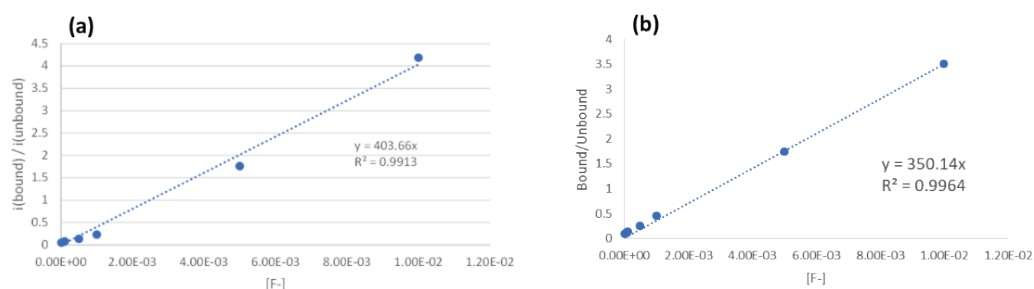
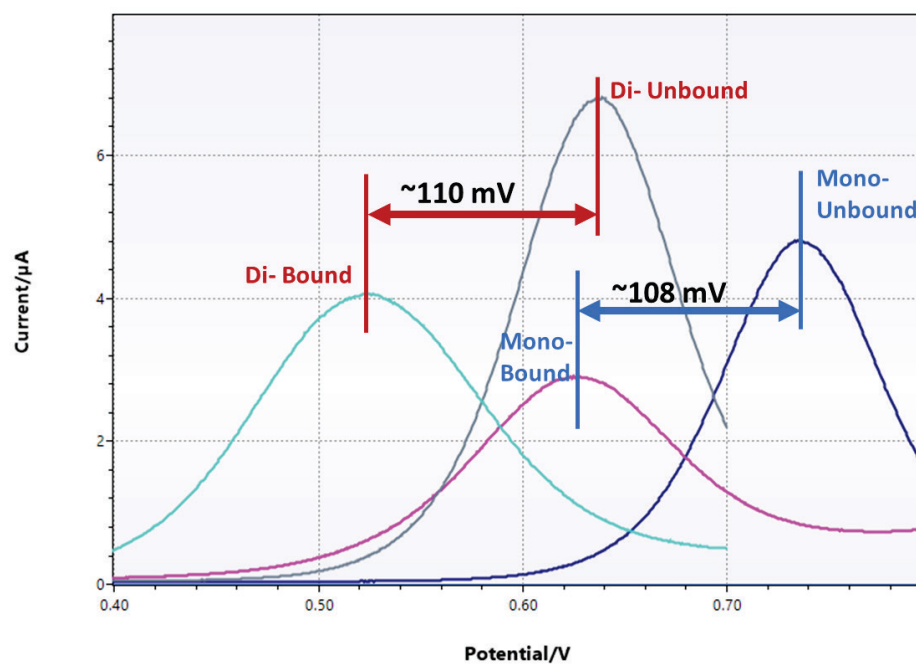


Table 1. Data obtained from the calibration curve for 1 and 2. Standard deviations were determined from \_10\_ samples/scans.

	Linear Range	Slope	R <sup>2</sup>	y-residuals (%)	LOD (μM)
<b>Mono-</b>	50 μM - 10 mM	350.13	0.9967	1.42E-03	12.2
<b>Di-</b>	50 μM - 10 mM	403.65	0.9909	2.28E-03	19.5

Furthermore, DPV showed that both compounds had almost equal voltage shifts for bound and unbound peaks, which might be due to both compounds binding one fluoride ion. This shift results from the change in electron density adjacent to the ferrocene core following fluoride binding. This phenomenon will be investigated using DFT simulations in future work.

Figure 20. Comparison of bound and unbound peaks obtained via DPV for 1 and 2.



## 4 Conclusions and Future work

In this work, we were able to successfully synthesize and purify di/mono boronic acid functionalized ferrocene which was capable of binding fluoride ions. The binding phenomenon was observed using NMR, fluorescent quenching, and electrochemical studies. Future work will show selectivity of these molecules in presence of potential interfering ions and extensive computational experiments to further confirm the mechanism of binding of these compounds. The detection of fluoride below the WHO limit of 1.5 mg/L with both fluorescence and electrochemical techniques has demonstrated the potential for this molecule to be a field-deployable sensing strategy.

## References

- Bresner, C., S. Aldridge, I. A. Fallis, C. Jones, and L. L. Ooi. 2005. "Selective electrochemical detection of hydrogen fluoride by ambiphilic ferrocene derivatives." *Angew. Chemie - Int. Ed.* 44 (23): 3606–3609. <https://doi.org/10.1002/anie.200500527>.
- De Silva, A. P., H. Q. N. Gunaratne, T. Gunnlaugsson, A. J. M. Huxley, C. P. McCoy, J. T. Rademacher, and T. E. Rice. 1997. "Signaling recognition events with fluorescent sensors and switches." *Chem. Rev.* 97 (5): 1515–1566. <https://doi.org/10.1021/cr960386p>.
- EPA. 2000. "Guide for industrial waste management protecting." *Ind. Waste Manag.* 1–478.
- Jang, Y. J., K. Kim, O. G. Tsay, D. A. Atwood, and D. G. Churchill. 2015. "Destruction and detection of chemical warfare agents." *Chem. Rev.* 115 (24): PR1–PR76. <https://doi.org/10.1021/acs.chemrev.5b00402>.
- Saleem, M.; H. Yu, L. Wang, Zain-Ul-Abdin, H. Khalid, M. Akram, N. M. Abbasi, and Y. Chen. 2016. "Study on Synthesis of Ferrocene-Based Boronic Acid Derivatives and Their Saccharides Sensing Properties." *J. Electroanal. Chem.* 763: 71–78. <https://doi.org/10.1016/j.jelechem.2015.12.028>.
- Shrivastava, A., and V. Gupta. 2011. *Chi Analytical Methods*.
- Yamamoto, H., A. Ori, K. Ueda, C. Dusemund, and S. Shinkai. 1996. "Visual sensing of fluoride ion and saccharides utilizing a coupled redox reaction of ferrocenylboronic acids and dye molecules." *Chem. Commun.* (3): 407–408. <https://doi.org/10.1201/9781315274508-20>.

## Acronyms and Abbreviations

3-APBA	3-Aminophenylboronic acid
CV	Cyclic voltammetry
DI	Deionized
DCM	Dichloromethane
DFT	Density-functional theory
EL	Environmental Laboratory
ERDC	Engineer Research and Development Center
EtOAc	Ethyl acetate
HOMO	Highest occupied molecular orbital
LOD	Limit of Detection
LUMO	Lowest unoccupied molecular orbital
M	Molarity
NMR	Nuclear magnetic resonance
PLE	Photoluminescence excitation
PM <sub>3</sub>	Parametric Method 3
RBF	Round-bottom flask
RT	Room Temperature
SWV	Square wave voltammetry
TBAF	Tetrabutylammonium fluoride
TBA-PF <sub>6</sub>	Tetrabutylammonium hexafluorophosphate
TEA	Triethylamine
THF	Tetrahydrofuran
UV-Vis	Ultraviolet–visible
WHO	World Health Organization



REPORT DOCUMENTATION PAGE				Form Approved OMB No. 0704-0188	
Public reporting burden for this collection of information is estimated to average 1 hour per response, including the time for reviewing instructions, searching existing data sources, gathering and maintaining the data needed, and completing and reviewing this collection of information. Send comments regarding this burden estimate or any other aspect of this collection of information, including suggestions for reducing this burden to Department of Defense, Washington Headquarters Services, Directorate for Information Operations and Reports (0704-0188), 1215 Jefferson Davis Highway, Suite 1204, Arlington, VA 22202-4302. Respondents should be aware that notwithstanding any other provision of law, no person shall be subject to any penalty for failing to comply with a collection of information if it does not display a currently valid OMB control number. PLEASE DO NOT RETURN YOUR FORM TO THE ABOVE ADDRESS.					
1. REPORT DATE (DD-MM-YYYY) 07/01/2022		2. REPORT TYPE Final Report		3. DATES COVERED (From - To)	
4. TITLE AND SUBTITLE Boronic Acid Functionalized Ferrocene Derivatives Towards Fluoride Sensing				5a. CONTRACT NUMBER	
				5b. GRANT NUMBER	
				5c. PROGRAM ELEMENT U452684	
6. AUTHOR(S) P. U. Ashvin Iresh Fernando, Gilbert K. Kosgei, Matthew W. Glasscott, Garrett W. George, Erik Alberts, and Lee C. Moores				5d. PROJECT NUMBER 496992	
				5e. TASK NUMBER A1000	
				5f. WORK UNIT NUMBER	
7. PERFORMING ORGANIZATION NAME(S) AND ADDRESS(ES) US Army Engineer Research and Development Center (ERDC) Environmental Laboratory (EL) 3909 Halls Ferry Rd Vicksburg, MS 39180-6199  Bennett Aerospace Inc. 1100 Crescent Green #250 Cary, NC 27518  SIMETRI 7005 University Blvd. Winter Park, FL 32792				8. PERFORMING ORGANIZATION REPORT NUMBER  ERDC/EL TR-22-7	
9. SPONSORING / MONITORING AGENCY NAME(S) AND ADDRESS(ES) Installation and Operational Environments 3909 Halls Ferry Rd. Vicksburg, MS 39180				10. SPONSOR/MONITOR'S ACRONYM(S)	
				11. SPONSOR/MONITOR'S REPORT NUMBER(S)	
12. DISTRIBUTION / AVAILABILITY STATEMENT Approved for public release; distribution is unlimited.					
13. SUPPLEMENTARY NOTES					
14. ABSTRACT In this technical report (TR), a robust, readily synthesized molecule with a ferrocene core appended with one or two boronic acid moieties was designed, synthesized, and used toward F <sup>-</sup> (free fluoride) detection. Through Lewis acid-base interactions, the boronic acid derivatives are capable of binding with F <sup>-</sup> in an aqueous solution via ligand exchange reaction and is specific to fluoride ion. Fluoride binding to ferrocene causes significant changes in fluorescence or electrochemical responses that can be monitored with field-portable instrumentation at concentrations below the WHO recommended limit. The F <sup>-</sup> binding interaction was further monitored via proton nuclear magnetic resonance spectroscopy ( <sup>1</sup> H-NMR). In addition, fluorescent spectroscopy of the boronic acid moiety and electrochemical monitoring of the ferrocene moiety will allow detection and estimation of F <sup>-</sup> concentration precisely in a solution matrix. The current work shows lower detection limit (LOD) of ~15 µM (285 µg/L) which is below the WHO standards.  Preliminary computational calculations showed the boronic acid moieties attached to the ferrocene core interacted with the fluoride ion. Also, the ionization diagrams indicate the amides and the boronic acid groups can be ionized forming strong ionic interactions with fluoride ions in addition to hydrogen bonding interactions.					
15. SUBJECT TERMS Military bases                                      Waste products                                      Boronic acid Environmental protection                      Fluorides – Ions – Detection                      Ferrocene					
16. SECURITY CLASSIFICATION OF:			17. LIMITATION OF ABSTRACT	18. NUMBER OF PAGES	19a. NAME OF RESPONSIBLE PERSON
a. REPORT Unclassified	b. ABSTRACT Unclassified	c. THIS PAGE Unclassified			19b. TELEPHONE NUMBER (include area code)

